

# OPTIMAL DESIGN OF AN ACTIVE TWIST 1:2.5 SCALE ROTOR BLADE

Pierangelo Masarati<sup>†‡</sup>, Marco Morandini<sup>‡</sup>, Johannes Riemenschneider<sup>§</sup>, Peter Wierach<sup>§</sup>,  
Sergej Gluhikh<sup>¶</sup>, Evgeny Barkanov<sup>¶</sup>

<sup>‡</sup>Politecnico di Milano  
Milano, Italy

<sup>§</sup>DLR  
Braunschweig, Germany

<sup>¶</sup>Riga Technical University  
Riga, Latvia

## Abstract

This paper presents preliminary results about the design and optimization of a model-scale active twist blade actuated by means of Macro Fiber Composites (MFC), as part of the EU-sponsored Friendcopter project for an environmentally friendly helicopter. The capability to numerically characterize induced strain composite beam sections is used in an optimization problem to determine the design of the rotor blade, which will be subsequently experimented in a hover test rig at DLR.

## Nomenclature

---

$EA$	tension stiffness
$EJ_y$	beamwise bending stiffness
$EJ_z$	chordwise bending stiffness
$GA_y$	chordwise shear stiffness
$GA_z$	beamwise shear stiffness
$GJ$	torsional stiffness
$M_i$	$i$ -th internal moment component
$T_i$	$i$ -th internal force component
$\epsilon_i$	$i$ -th linear strain component
$\kappa_i$	$i$ -th angular strain component
C.G.	center of gravity
S.C.	shear center
T.C.	tension center

---

## Introduction

Friendcopter is a EU-sponsored research project aimed at investigating the feasibility and the possible development trends for an environmentally friendly helicopter. It addresses different aspects of helicopter design and operation, including the use of appropriate trajectories when operating in ground proximity, the reduction of interior cabin noise, the quality of the emissions from engine exhausts and more. Work Package 5 specifically addresses the investigation of active control techniques applied to the rotor, to simultaneously reduce the vibrations transmitted to the airframe and the aerodynamic noise generated by the

rotor blades in certain flight regimes, and to improve the overall performances of the helicopter.

As the three objectives, although in general pursued in different flight regimes, may be contrasting and difficult if not impossible to achieve by means of a single active control principle, the partners agreed on investigating different, possibly complementary active control solutions according to a staggered approach. The idea is to investigate relatively consolidated, low risk techniques, which will be implemented in experimental setups, and, at the same time, higher risk solutions, which may not immediately turn into a successful experiment within the scope of this project but are likely to lead to an innovation in future helicopter design.

In the spirit of pursuing relatively consolidated active control techniques, the research team led by Deutsches Zentrum für Luft- und Raumfahrt (DLR), with the participation of Politecnico di Milano (POLIMI) and Riga Technical University (RTU), is currently investigating an innovative active blade twist solution based on the use of the next generation piezoelectric actuation concepts in conjunction with specifically tailored blade and blade section designs.

As highlighted in previous works conducted by DLR in conjunction with ONERA in the Active Twist Blade (ATB) project [1], state of the art Macro Fiber Composites [2, 3, 4] represent a promising solution for the implementation of active blade twist. In the course of the project it is planned to incorporate new technologies that are currently under development in other work packages of Friendcopter. These technologies are aiming at the exploitation of advanced piezoceramic multilayer technology for the design of low-profile in-plane actuation systems and will utilize the

---

Presented at the 31<sup>st</sup> European Rotorcraft Forum  
Florence, Italy, September 13–15 2005

<sup>†</sup>Corresponding author; via La Masa 34, 20156 Milano, Italy. Tel: +39 02 2399 8309. Fax: +39 02 2399 8334. email: pierangelo.masarati@polimi.it

piezoelectric  $d_{33}$  effect at significantly reduced actuation voltages.

As the number of parameters that may affect the general performances of the blade, and specifically those related to the active twist, is quite large, an important role in this work is played by automatic structural and multidisciplinary optimization.

### Approach

The comprehensive analysis of the aeroelastic behavior of helicopter blades typically relies on the beam model, which represents a usually accepted trade-off between accuracy and computational efficiency. The relatively simple structural and topological beam model can capture the complex behavior of very sophisticated induced strain, anisotropic and non-homogeneous rotor blades when appropriate elastic, inertial and piezoelectric beam section properties are available. The elastic/induced strain beam model is characterized first by a mix of general FEM and dedicated formulations [5]. The resulting section properties are directly used in the design and optimization at the section level. These properties are fed as input to the eigenanalysis of the blade and to the intrinsic beam model used in the aeroservoelastic analysis of the rotor in a related part of the project [6].

The design of an optimal active twist blade is logically split in two levels. At the rotor blade level optimal beam section properties are determined, while at the beam section level the beam section design parameters are sought that match the overall properties while complying with manufacturing and possibly cost constraints.

In the current state of the project, no rotor blade level optimization is being performed yet, but the blade is required to fit into some specified ranges of the design performance indices of the corresponding reference passive blade within a given tolerance, while maximizing the actuation authority per unit span, namely the torsion per unit applied voltage. More sophisticated design layouts will be considered at the blade level, including a non-uniform blade design that matches the overall passive properties of the original blade while allowing a higher freedom in the design of its active strain portion: a combination of active and passive spanwise portions of blade would allow to relax structural and aeroelastic constraints on the active portion of the blade. Further activity will include aeroservoelastic verification and, if required, further aeroservoelastic optimization of the blade and of the actuation system.

### Objective

The ultimate goal of the optimization process is to develop an optimal design and placement of the active plies in the rotor blade with respect to vibration reduction, aerodynamic noise abatement and performance improvement [7]. The complexity of the procedure required to compute the objective function, based on the interaction of many different software components (automatic discretization and mesh generation, blade section characterization, constraint evaluation by means of FEM/multibody analysis) suggests to adopt a multilevel optimization approach, otherwise the direct effect of changes in the design parameters on the objective function and on the constraints can be masked by the “noise” related to the computation, thus deceiving the optimization procedure.

In the present work, intermediate objectives are selected, whose local optimality is assumed to be beneficial in view of the global optimality of the overall design. Particular emphasis is put on maximizing the amplitude of the static induced blade twist per unit length, and on some spanwise weighted integral of the static induced twist, preserving as much as possible the dynamic properties of the passive blade, under the assumption that the dynamic response of the blade torsion, and thus the resulting perturbation of the aerodynamic forces, is maximized as well in the frequency interval of interest for the active control of the rotor. Figure 1 sketches the parametric discretization of the blade section that is being optimized. Actually, that figure refers to an initial, tentative design that evolved in more specialized layouts, with the active plies placed directly on the outer surface of the blade in single or multiple patches, as illustrated in the following.

### Induced Strain Blade Section Characterization

The blade section elastic and piezo-electric characterization is fundamental to obtain realistic estimates of the induced strain capabilities of a design. Even the characterization of passive rotor blades may represent a challenge because the section presents many different layers and portions, made of different, heterogeneous anisotropic materials. As a consequence, simple analysis approaches may lead to inconsistent results in terms of elastic properties, because the anisotropy of the materials and the complex geometry of the section typically lead to section properties with couplings that cannot be described by the conventional engineering properties.

The approach followed by DLR is based on 3D FEM modeling of a blade section using ANSYS. A paramet-

Materials:

- UD GFRP
- Foam
- MFC
- ±45° GFRP

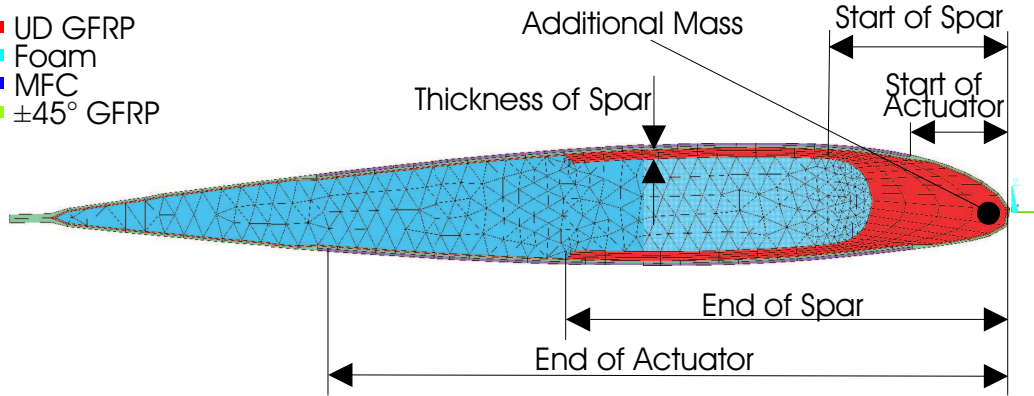


Figure 1: Active Twist Blade section.

ric model generator was established in ANSYS Parametric Design Language (APDL). That way models with different values for the design parameters can be generated automatically. Foam, spar, skin and MFC actuator were modeled with SOLID45 elements, in order to make the model more accurate. Additional balancing weight was introduced as point masses MASS21 in the spar. The level of discretization in the cross-section plane is illustrated in Figure 1. The piezoelectric coupling effect is modeled by exploiting the thermal analogy. In several test cases this procedure was compared with the approach by POLIMI. The results obtained with both methods were in good agreement. In a second step the global stiffness and inertia terms are derived and applied to a beam model for the eigenfrequency analysis.

POLIMI follows an approach based on a 2D finite element model of the section, which allows a level of detail comparable to that used by DLR. The model is used to define the geometry of the beam section and to solve the linear elastic problem on the 2D domain of the beam section for load distributions that correspond to unit internal forces and applied electric voltage and account for the appropriate natural boundary conditions. As a consequence, the solution is intrinsically compatible, because of the displacement-based FEM modeling of the continuum, while the local equilibrium is enforced in a weak form [5]. A clear advantage of this approach is that inter- and intra-domain strains and stresses can be computed with the desired level of accuracy by refining the mesh.

RTU follows yet another approach, based on 3D FEM modeling of a portion of blade using ANSYS, as illustrated in Figure 2. The rotor blade skin and the rear portion of the spar are modeled by linear layered

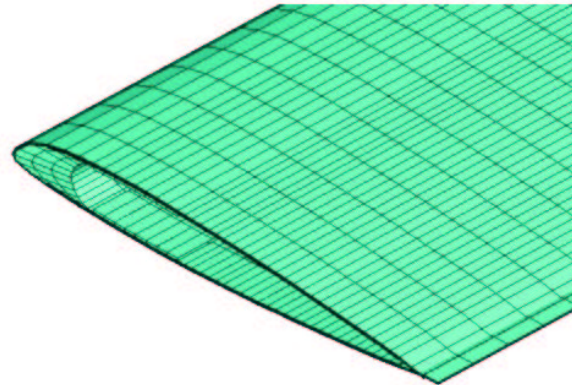


Figure 2: Active Twist Blade FEM model.

structural shell elements SHELL99, while the foremost portion of the spar and the foam are modeled by 3D 20 node structural solid elements SOLID186. To preserve the outer shape and geometry of the airfoil, the layered elements are offset inward from the external contour, where the nodes are placed.

Before starting the analysis, convergence tests of the finite element results have been examined for different meshes. As a consequence of the complexity of the structure investigated, three separate convergence problems have been solved for components of the rotor blade; the skin, the spar and the foam.

When dealing with isotropic, uniform straight beams, the stiffness matrix of the section can be partitioned in axial and transverse load carrying portions

$$\begin{Bmatrix} T_x \\ M_y \\ M_z \end{Bmatrix} = \begin{bmatrix} A_{11} & A_{12} & A_{13} \\ A_{12} & A_{22} & A_{23} \\ A_{13} & A_{23} & A_{33} \end{bmatrix} \begin{Bmatrix} \epsilon_x \\ \kappa_y \\ \kappa_z \end{Bmatrix} \quad (1)$$

$$\begin{Bmatrix} T_y \\ T_z \\ M_x \end{Bmatrix} = \begin{bmatrix} S_{11} & S_{12} & S_{13} \\ S_{12} & S_{22} & S_{23} \\ S_{13} & S_{23} & S_{33} \end{bmatrix} \begin{Bmatrix} \epsilon_y \\ \epsilon_z \\ \kappa_x \end{Bmatrix} \quad (2)$$

where  $T_i$  and  $M_i$  are the internal forces and moments,  $\epsilon_i$  and  $\kappa_i$  are the linear and angular strains of the beam, and  $A_{ij}$  and  $S_{ij}$  are the stiffness coefficients related to axial and shear straining of the beam section.

These coefficients can be factored out to yield the well-known engineering parameters, i.e. two distinct reference systems representing the tension and the shear centers, and the axial and shear elastic properties referred to these two locations, in the principal directions. These properties can be consistently obtained from a simple, geometry-based analysis.

However, for anisotropic, non-homogeneous beam sections, the axial and the transverse behavior of the beam no longer can be separated; the stiffness matrix becomes fully coupled, and even the tension and the shear center lose their meaning.

This should be taken into account when analyzing the dynamic and aeroelastic behavior of the rotor; in fact, the 6 by 6 stiffness and inertia matrices resulting from the beam section analysis, plus, for  $N_p$  piezo actuators, the 6 by  $N_p$  piezoelectric coupling matrix, are directly fed to the multibody aeroservoelastic analysis that is used to assess the active rotor design. If required, rotorcraft aeroservoelastic analysis will be part of the outer optimization level.

#### Blade Section Optimization Procedure

As already anticipated, the objective is to maximize the twist per unit span per unit electric field of a uniform beam section, under a given set of constraints.

Most of the constraints result from the need to match as close as possible the properties of the reference passive design, to reduce the likelihood of the insurgence of dynamics and aeroelastic issues, so that this level of optimization can be run standalone. Some of the constraints actually result from manufacturing considerations of from the need to keep the number of design variables under a reasonable threshold. The constraints are:

- a) the outer shape is that of a given airfoil (NACA 23012 in the present case);
- b) the spar is "C" shaped; the thickness of the rear portion of the "C" is constant; it ends with a triangular shape, while the front fitting is circular;
- c) a lead ballast with circular shape is buried in the

front portion of the "C" spar; it does not carry tension;

- d) the chordwise location of the C.G. is between 22% and 30% of the chord;
- e) the chordwise location of the elastic axis is between 20% and 25% of the chord;
- f) the mass per unit span of the cross section must be below a given value;
- g) the first torsional eigenfrequency at nominal RPM must be between 3.5/rev and 4/rev;
- h) the maximum axial strain in the "C" spar is limited;
- i) the beamwise bending stiffness must be between a lower and an upper limit;
- j) the torsional stiffness must be above a limit value;

Slightly different sets of design variables have been considered by the partners, to further expand and explore the design space.

DLR focused on the parametric investigation, required for the optimization procedure developed by RTU. The effects of different design parameters on the properties of the blade sections were discussed using an initial FE model of the section. The model consists of two MFC actuators (thickness 0.3 mm each), one on the upper and one on the lower side of the blade section. The skin consists of two layers: an outer layer of  $\pm 45$  deg GFRP (thickness 0.25 mm) and an inner layer of 0 deg (unidirectional, spanwise) GFRP (thickness 0.125 mm). The spar is modeled with 0 deg GFRP as well. Additional weight in the nose has the mass of 182.5 g/m, located 1.5 mm behind the leading edge. This mass was not changed during the investigation. The parameters addressed are:

- D.1) the leading location of the MFC actuator;
- D.2) the chordwise length of the MFC actuator;
- D.3) the thickness of the "C" spar;
- D.4) the length of the "C" spar.

The cross section was modeled in ANSYS in order to determine the cross sectional properties of the design. The general geometry and the stacking of the different materials are illustrated in Figure 1.

The influence of the size of the induced strain actuator has been investigated by varying the length of the patch for three starting points: 10%, 20% and 30% of the chord from the leading edge, with the end

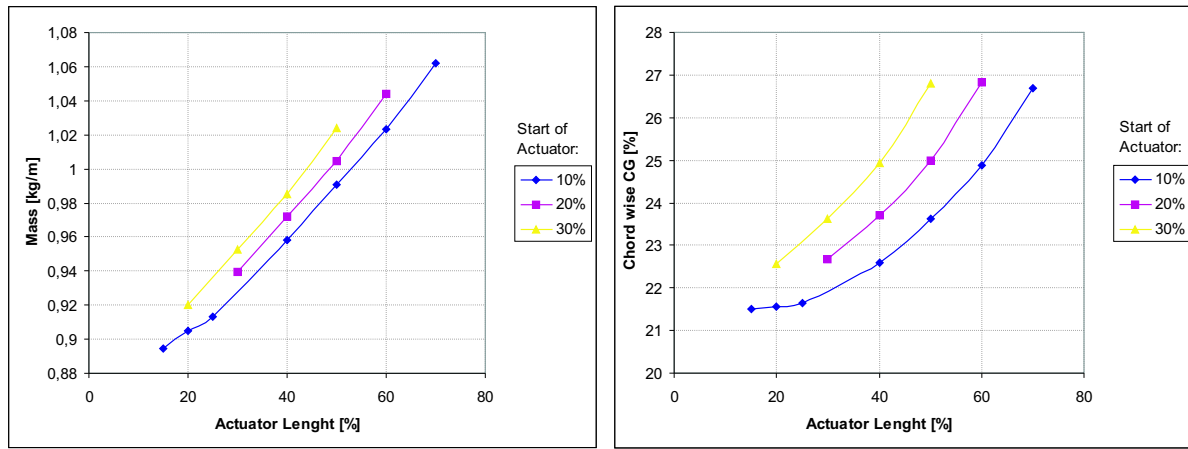


Figure 3: Sensitivity of mass (left) and C.G. chordwise location (right) to chordwise actuator extension and position.

of the spar set to 40% of the chord and its thickness set to 1 mm. Figure 3 illustrates the sensitivity of the total mass and of the C.G. of the section with respect to the chordwise actuator extension. The strong influence of the additional actuator mass is caused by the density of the MFC ( $4.7 \text{ g/cm}^2$ ), which is significantly high in comparison to the GFRP ( $2.008 \text{ g/cm}^2$ ) and foam ( $0.052 \text{ g/cm}^2$ ). The additional mass can be as high as 20% (compared to that of the passive blade) with just one MFC layer for the lower and upper skin, respectively. The closer the *Start of Actuator* point is located to the leading edge, the lower is the additional mass; this latter effect is rather small. The C.G. moves backward as the added mass increases. Figure 4 shows the influence of the same parameters on the bending stiffness in beam and chord direction. The stiffness increase in beamwise direction is stronger than that in chordwise direction. The farther back the active portion is located, the higher is the stiffness increase; this is caused, in the beamwise direction by the larger distance from the neutral axis of the piezoelectric material. When the actuator starts at 10% and spans up to 15% of the chord the beamwise stiffness slightly decreases as the actuator becomes longer. This is due to the fact that, in this configuration, the actuator is located in the front of the spar only; as a consequence, the piezoelectric material is replacing the GFRP material, whose stiffness is higher in the spanwise direction of the blade. The torsional stiffness ( $GJ$ ) and the first torsional frequency at nominal RPM are shown in Figure 5. The stiffness increases almost linearly with the chordwise actuator extension. For very short actuators, located in the region of the spar, a behavior analogous to that of the beamwise bending stiffness, where the stiffness

initially slightly decreases. The eigenfrequency shows a strong nonlinear behavior with respect to the chordwise actuator extension, but the change in magnitude is quite limited.

Figure 6 shows that the active twist is pretty much linear with the chordwise actuator extension. A small perturbation in the region of the rear end of the spar, which in the baseline design occurs at a chordwise actuator extension of 25%, distinctly appears on the plot on the right. This behavior strongly depends on the participation to the torsional stiffness of the spar, which the actuator has to counteract. The reduced authority of that portion of MFC patch suggests the opportunity to split the patch in two pieces in that position.

The influence of the spar length on the main properties of the section has been investigated while maintaining the beginning of the actuator at 10% of the chord, and varying its rear end from 70% to 80% of the chord; a thickness of 1 mm has been considered. Figure 7 shows the strong influence of the spar length on the mass and the C.G. of the section. The mass increases linearly with the spar length, while the C.G. shift shows a nonlinear behavior. Figure 8 shows the influence of the spar length on the bending stiffness in both directions. The increase in stiffness in the beamwise direction is much stronger than that for the chordwise direction. The beamwise bending stiffness increases almost linearly, while the lag wise stiffness shows a nonlinear trend. The active twist and the torsional stiffness ( $GJ$ ) are shown in Figure 9. The strong dependence of the twist on the torsional rigidity is apparent, with a remarkable nonlinear behavior around 40% of the chord when the end of the actuator is located at 70% of the chord. No satisfactory

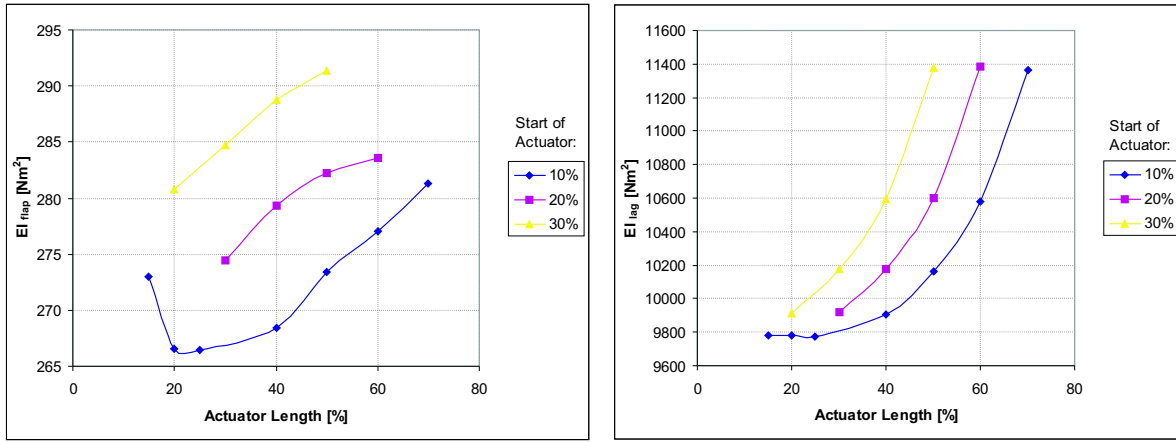


Figure 4: Sensitivity of beam (left) and chord (right) bending stiffness to chordwise actuator extension and position.

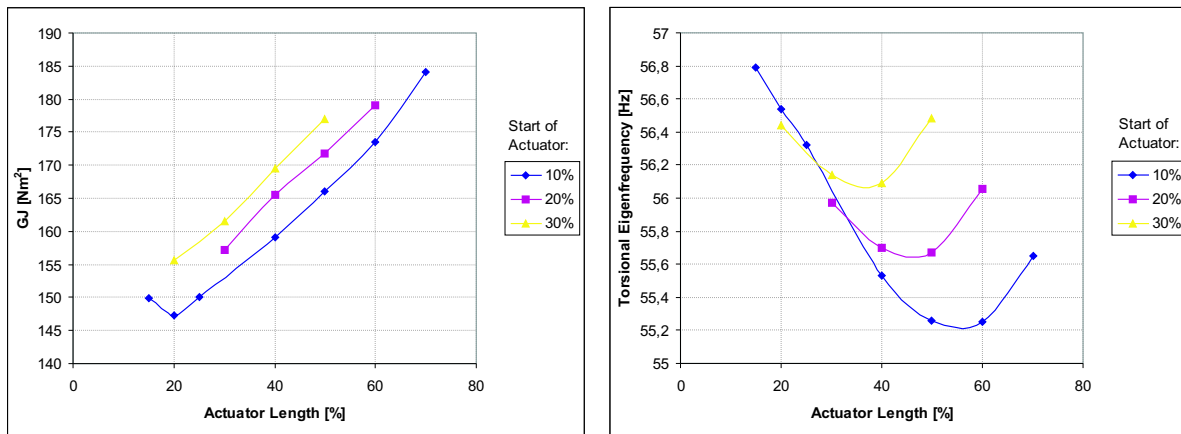


Figure 5: Sensitivity of torsional stiffness (left) and of nominal RPM 1<sup>st</sup> torsional eigenfrequency (right) to chordwise actuator extension and position.

explanation for this behavior has been found yet. The influence of the spar length on the first torsional eigenfrequency at nominal RPM is shown in Figure 10. The increase in polar inertia is clearly dominating the increase in torsional stiffness.

The influence of the thickness of the rear portion of the spar has been investigated while keeping the end of the spar at 40% of the chord, and the beginning and the end of the piezoelectric patch at 10% and 80% of the chord, respectively. Figure 11 shows that the mass increases linearly when the thickness of the rear portions of the “C” spar is increased, while the C.G. moves toward the leading edge, since most of the spar material is located in front of the 25% line. All stiffnesses increase with the spar thickness, as illustrated in Figure 12 and in Figure 13 (left). The active twist again depends on the torsional stiffness,

as illustrated in Figure 13 (right). The reason for the deviation from linearity is related to the interaction of the MFC patch with spar rear end region. The torsional stiffness (Figure 13 left) does not change significantly with the spar thickness, but the polar inertia does. As a consequence, the first torsional frequency at nominal RPM decreases significantly when the spar thickness increases, as illustrated in Figure 14.

POLIMI performed the optimization of the blade section with the previously described constraints using a standard Sequential Quadratic Programming toolbox, considering as design variables:

- P.1) the chordwise position where the piezoelectric patch starts;
- P.2) the length of the piezoelectric patch;

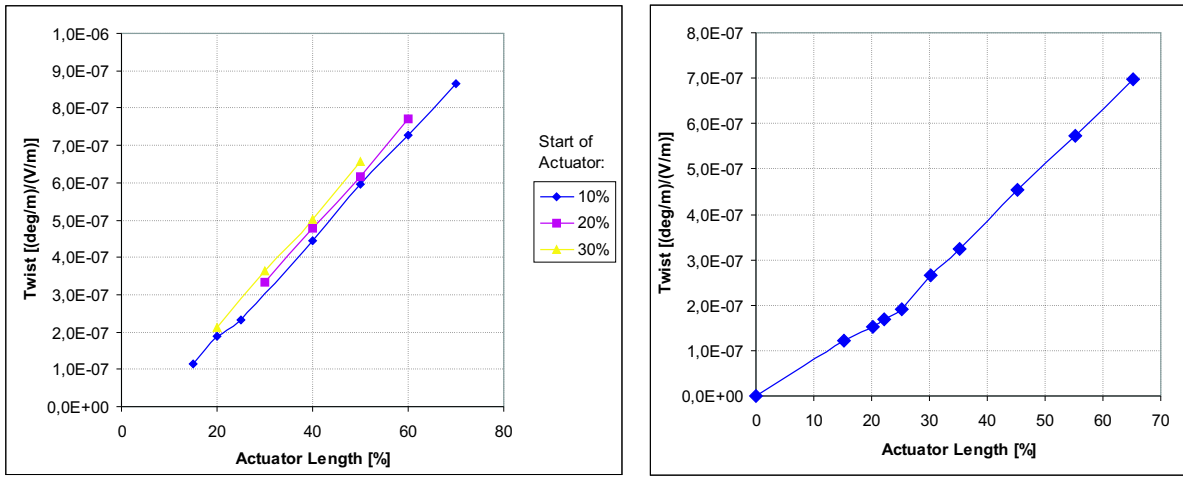


Figure 6: Sensitivity of active twist to chordwise actuator extension and position (left); sensitivity to chordwise actuator extension with different spar material (right).

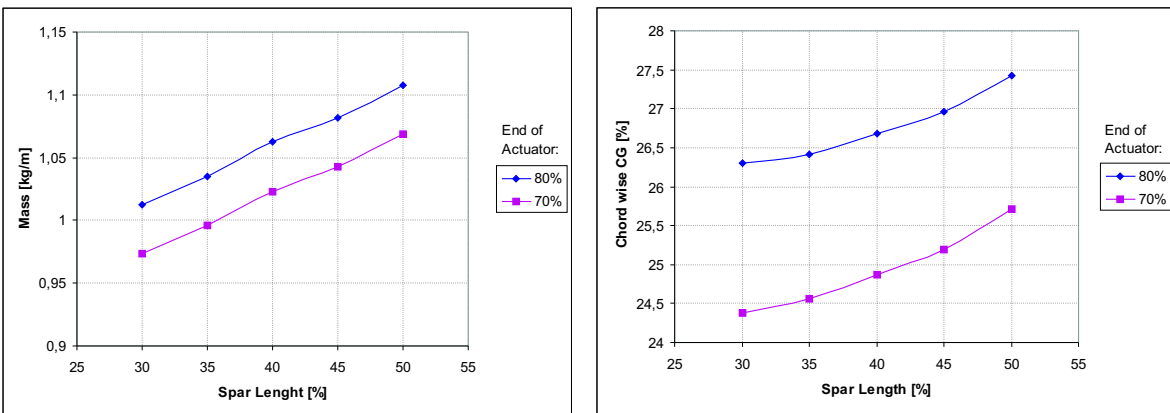


Figure 7: Sensitivity of mass (left) and C.G. chordwise position (right) to spar length.

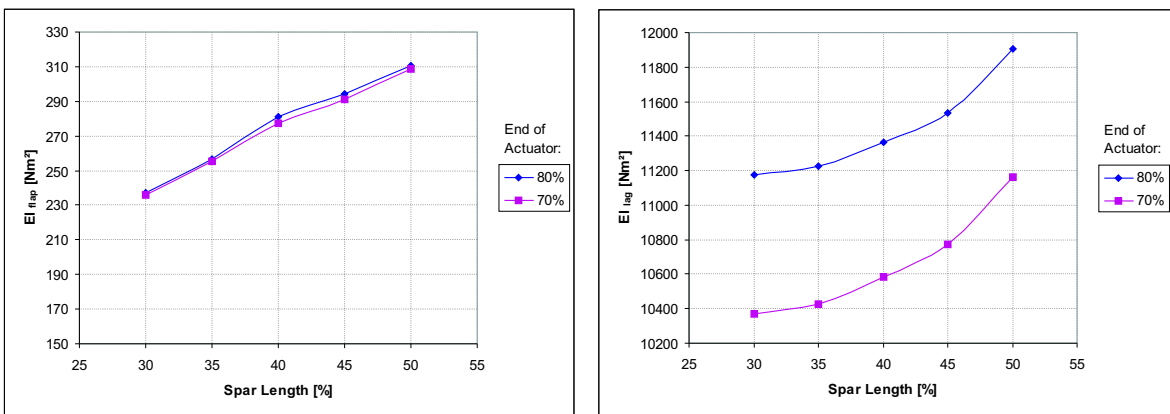


Figure 8: Sensitivity of beamwise (left) and chordwise (right) bending stiffness to spar length.

P.3) the thickness of the piezoelectric patch;

P.4) the radius of the balancing mass;

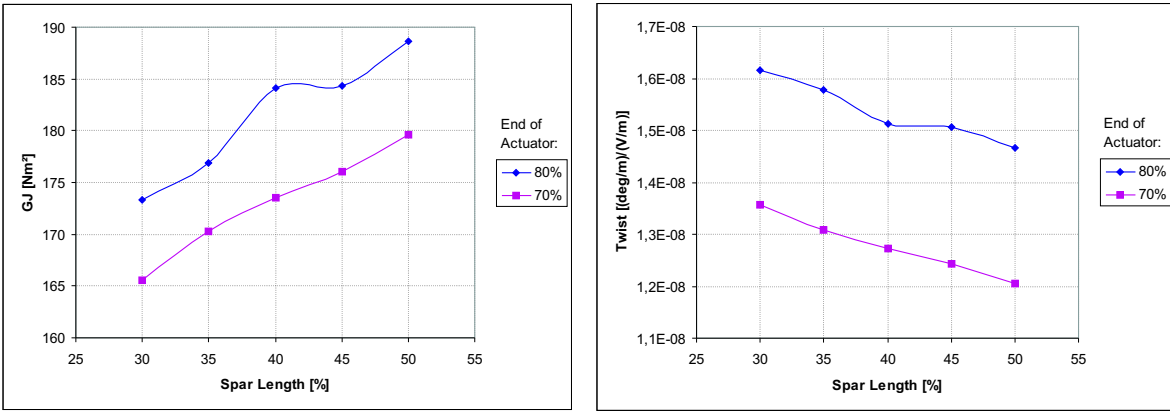


Figure 9: Sensitivity of torsional stiffness (left) and active twist (right) to spar length.

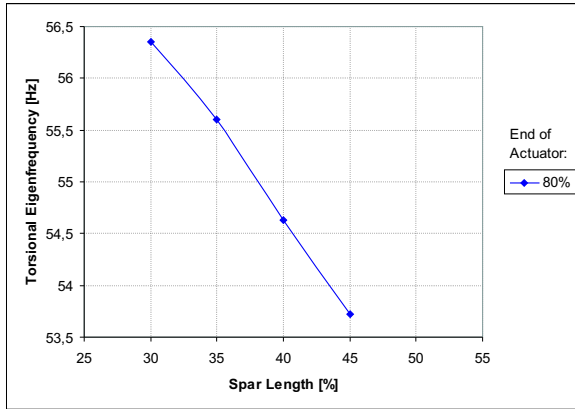


Figure 10: Sensitivity of nominal RPM 1<sup>st</sup> torsional frequency to spar length.

Table I: Best blade section optimization with the default constraints.

	Initial	Final	
Tension stiff.	61.02	86.16	% ref.
Chord shear stiff.	68.68	70.50	% ref.
Beam shear stiff.	6.94	13.47	% ref.
Torsional stiff.	156.09	163.28	% ref.
Beam bend. stiff.	93.10	107.90	% ref.
Chord bend. stiff.	226.78	266.72	% ref.
Mass	93.47	131.36	% ref.
Twist inertia	135.51	178.84	% ref.
Beam inertia	98.64	137.90	% ref.
Chord inertia	136.37	179.79	% ref.
Chord $\Delta$ C.G.	4.71	4.88	% chord
Chord $\Delta$ SC	0.04	-0.57	% chord
Chord $\Delta$ T.C.	11.77	7.36	% chord
Authority	20.59	100.00	%

P.5-8) four parameters that define the geometry of the “C” spar.

The model is made of an outer layer of  $\pm 45$  deg fabric, with the orthotropic piezoelectric patches bonded on the outer face and the gaps filled with epoxy. The spar is modeled by automatically generating the desired shape, according to the design variables that define the position and the shape of the rear portion, the thicknesses and the location of the circular fitting of the front. A circular inclusion representing the lead balancing mass is considered as well; its stiffness properties have been modified to account for the correct inplane stiffness, while eliminating its participation to the spanwise stiffness. The rest of the inner section has been filled with foam. preliminary analyses showed that neglecting the foam leads to small differences in terms of stiffness, but may lead to significant variations in the position of the elastic axis.

Note that the thickness of the MFC patch, param-

eter (P.3), should be imposed by technological constraints; however, since that component will be specifically manufactured for the present test, it has been considered a design variable to assess its impact on the optimality of the design. On the contrary, the thickness of the  $\pm 45$  deg fabric that wraps the airfoil has been enforced. Currently, the constraint (g) on the torsional frequency has been accounted for by considering the analytical frequency of a uniform beam of appropriate length without any elastic or inertial twist-bending coupling. A more accurate eigenanalysis of the fully coupled, rotating blade will be accounted for in future optimizations.

Figure 15 illustrates the initial and the best final design that has been obtained so far. Table I illustrates some relevant figures about the same two blade designs as compared to those of the reference passive rotor blade. Note that Table I does not describe the

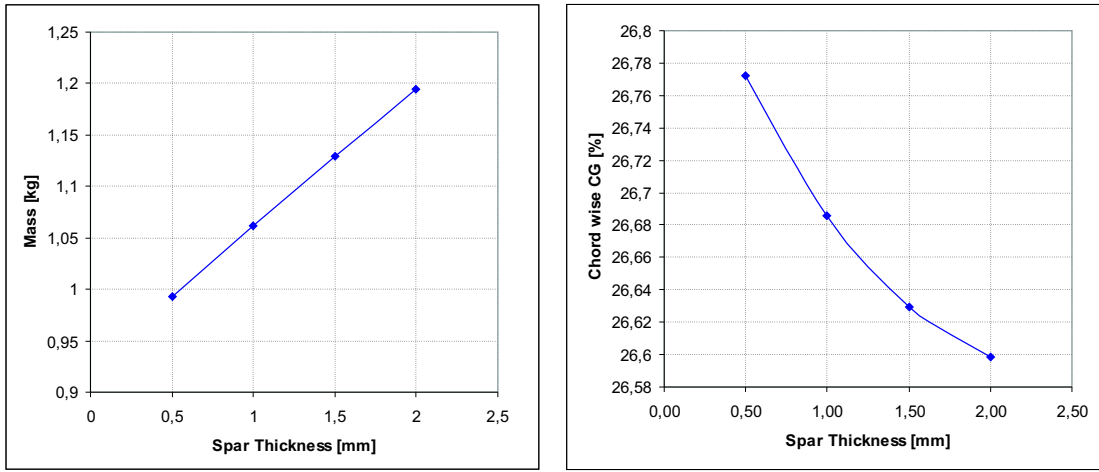


Figure 11: Sensitivity of mass (left) and C.G. chordwise location (right) to spar thickness.

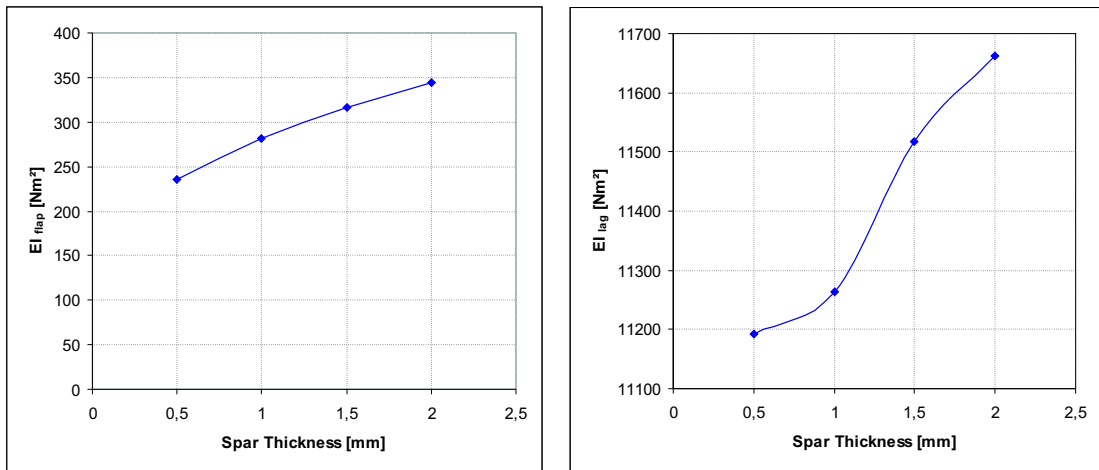


Figure 12: Sensitivity of beamwise (left) and chordwise (right) bending stiffness to spar thickness.

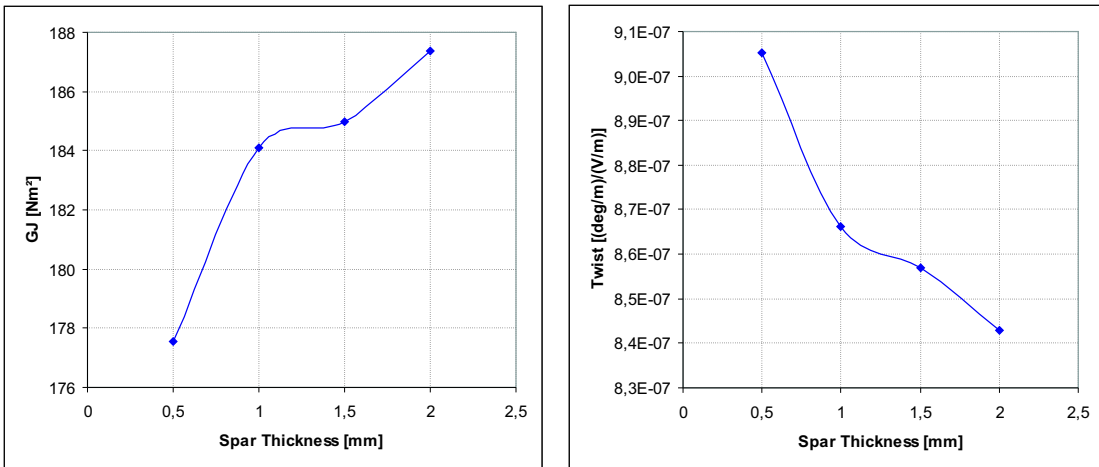


Figure 13: Sensitivity of torsional stiffness (left) and active twist (right) to spar thickness.

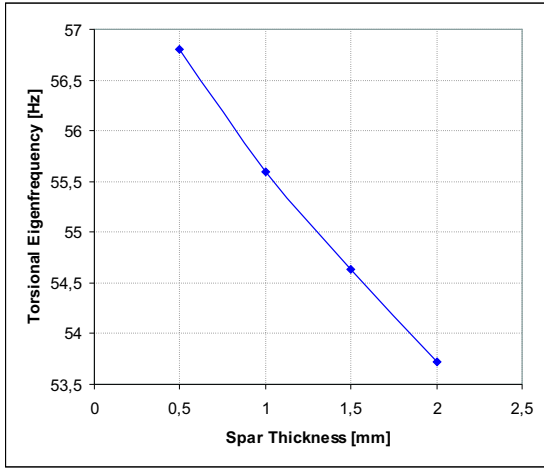


Figure 14: Sensitivity of nominal RPM 1<sup>st</sup> torsional frequency to spar thickness

couplings of the active twist blade section, which are not covered by the conventional engineering properties.

The resulting design gives very significant performances in terms of active twist capability per unit electric field in the MFC:  $1.04 \cdot 10^{-6}$  (deg/m)/(V/m); this figure has been increased by the optimization about 5 times with respect to that of the initial configuration. When an electric field in the range of  $10^6$  V/m is applied, either by using a high voltage or a very small electrode distance, a static actuation above 1 deg/m is expected.

However, from a helicopter blade design point of view, the resulting design may suffer from allowing the MFC to carry too much of tension, bending and torsion, although all constraints are satisfied, and from allowing too large a separation between the center of gravity (C.G.) and the normal stresses center, or tension center (T.C.) on one side, and the shear center (S.C.) on the other side. As a consequence, further optimization attempts, with additional constraints, have been performed.

When independent constraints on the position of the C.G. and of the S.C. are considered, the former tends to move to the rearmost allowed position, while the latter moves straight to the foremost position, as indicated in Figure 15 and in Table I, where the distance between the two points results in 10% of the chord.

When an additional constraint on the relative distance between these two points is considered, less performing but more aeroelastically realistic blade sections result. Figure 16 illustrates the results of two optimizations with the additional constraint:

Table II: Blade section optimization with an additional constraint on C.G.-S.C. distance.

	8% chord	5% chord	
Tension stiff.	65.86	74.69	% ref.
Chord shear stiff.	62.06	51.46	% ref.
Beam shear stiff.	8.39	12.64	% ref.
Torsional stiff.	145.65	128.99	% ref.
Beam bend. stiff.	86.19	87.02	% ref.
Chord bend. stiff.	233.79	226.01	% ref.
Mass	107.02	103.28	% ref.
Twist inertia	151.53	138.03	% ref.
Beam inertia	110.16	88.25	% ref.
Chord inertia	152.50	139.19	% ref.
Chord $\Delta$ C.G.	4.84	1.30	% chord
Chord $\Delta$ S.C.	1.31	0.67	% chord
Chord $\Delta$ T.C.	8.77	5.10	% chord
Authority	74.37	33.05	% Tab. I

- k) the distance between the C.G. and the S.C. must be below a given fraction of the chord.

When its value is set to 8 and 5%, the actuation authority respectively reduces to 3/4 and 1/3 of the value obtained earlier, as indicated in Table II.

RTU focused on the effects of the number and placement of the MFC patches on the twist actuation authority, and on other parameters of the blade section, like the radius and location of the circular fitting in the nose of the “C” spar. To be able to formulate an optimization problem, a parametric study has been initially conducted. The dependence of the behavior functions (torsion angle, first torsion frequency, center of gravity, mass of cross section, bending and torsion stiffnesses, tension microstrains) on:

- R.1) the length of the rear portion of the spar;
- R.2) the thickness of the rear portion of the spar;
- R.3) the radius of the spar circular fitting;
- R.4) the chordwise length of the MFC patch;
- R.5) the thickness of the skin; and
- R.6) the voltage

has been studied.

The thickness of the rear portion of the spar shows quite a small influence on the behavior functions, while the chordwise length of the MFC patches shows the most significant influence on most of them, as expected. As a consequence, additional investigations

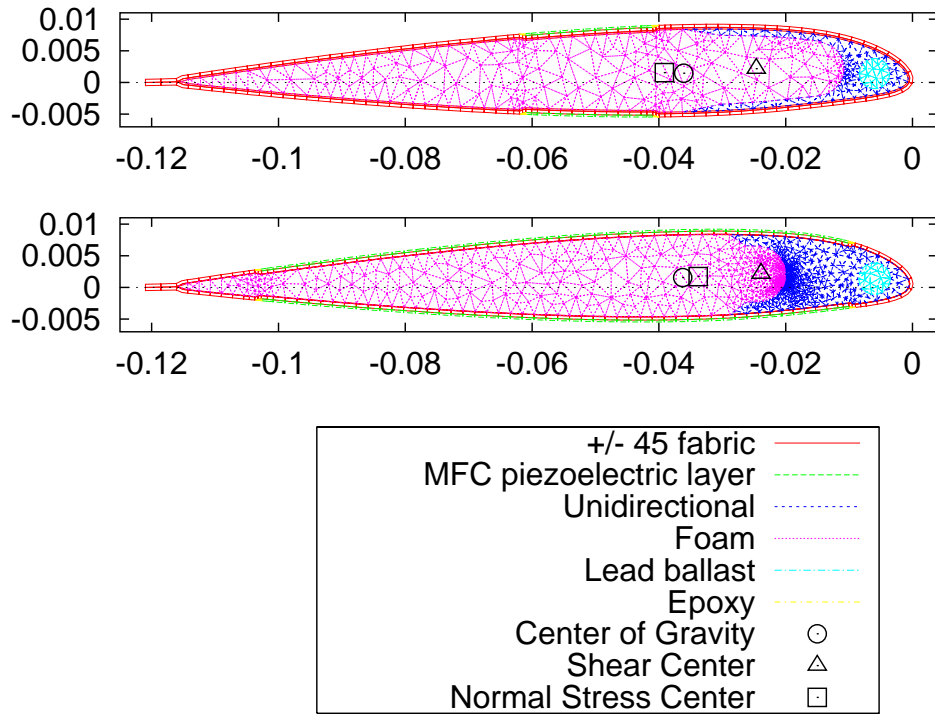


Figure 15: Blade section optimization with the default constraints: initial (top) and final (bottom) configuration. Properties are detailed in Table I.

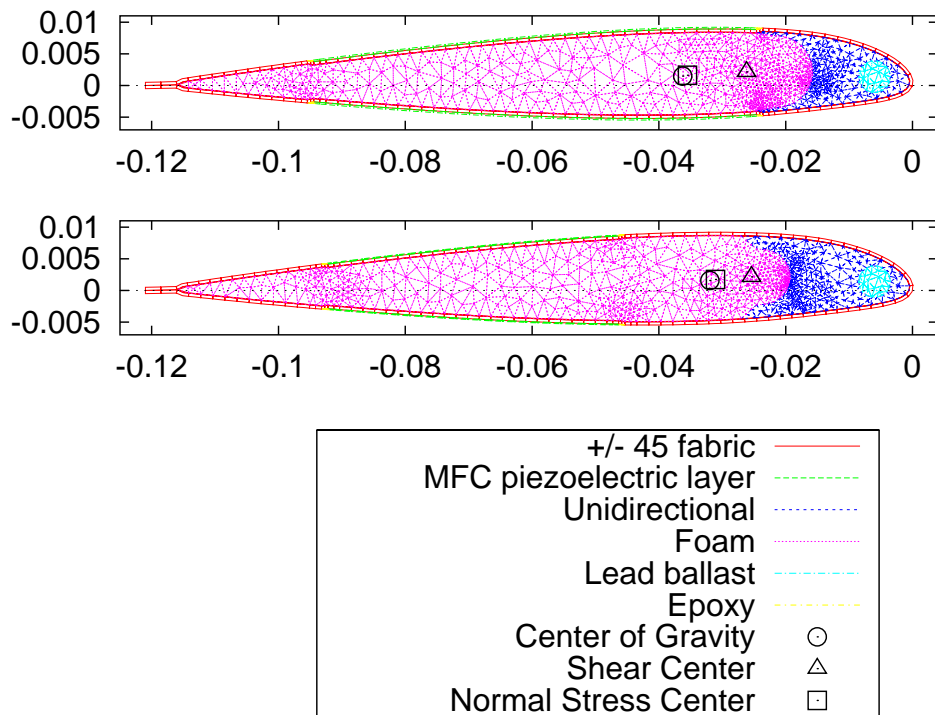


Figure 16: Blade section optimization with an additional constraint on C.G.-SC distance: 8% chord (top) and 5% chord (bottom). Properties are detailed in Table II.

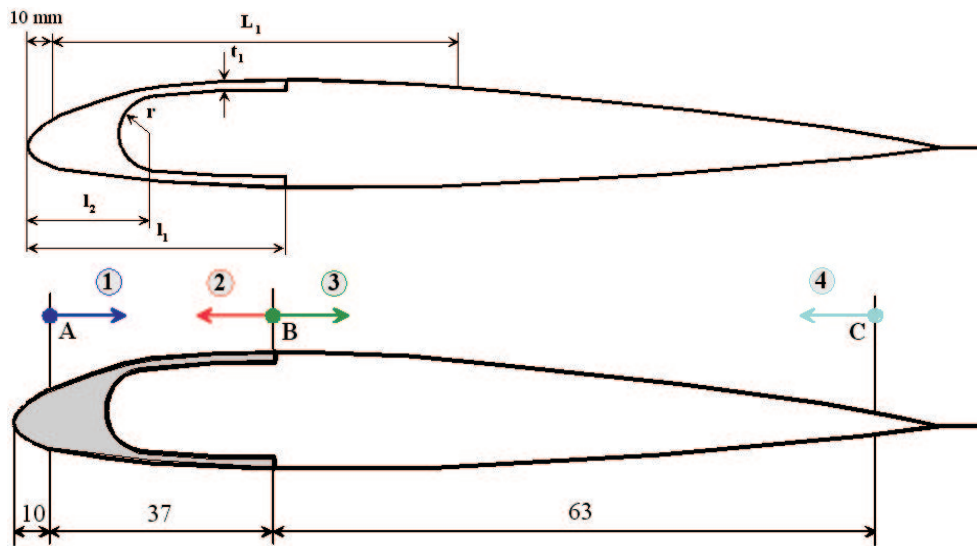


Figure 17: Sketch of the section geometry (top) and gluing patterns (bottom).

have been conducted to gain more insight into the influence of MFC chordwise length on the blade torsion angle.

Figure 6 shows that there appears to be a change in the slope of the torsion angle as soon as the MFC patch extends past the end of the “C” spar. This feature can be exploited to study the optimal location of the MFC in the rotor blade. For this reason, four separate problems have been solved, according to the symbols indicated in Figure 17:

1. MFC extending from A to B;
2. MFC extending from B to A;
3. MFC extending from B to C;
4. MFC extending from C to B.

Figure 18 illustrates the dependence of the torsion angle on the length of the MFC patch according to the four problems above, for a finite portion of blade 1.52 m long and for an applied voltage of 1000 V; curve (1) is analogous to those in Figure 6.

Figure 18 gives the possibility to choose an optimal strategy for MFC gluing in the rotor blade chord-wise direction. Clearly, for a given chordwise actuator extension, case 3, consisting in gluing the MFC patch right behind the end of the spar, appears to be optimal in terms of actuation authority per unit extension of the patch; the authority for a given size of the MFC patch is maximized when the solutions (2) and (3) are used simultaneously, limiting case (2) to 20÷25% of the chord.

Figure 19 illustrates the dependence of mass, C.G. location, active twist and nominal RPM first torsional

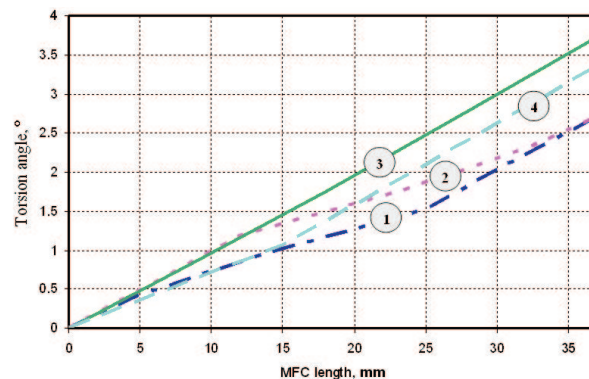


Figure 18: Dependence of torsion angle on MFC chordwise length and gluing pattern.

frequency of the blade as functions of the chordwise position of the circular fitting in the “C” spar. The behavior of the active twist slope with respect to the chordwise actuator extension and position initially highlighted by RTU in Figure 18 has been consistently observed by all partners, as appears from DLR results in Figure 5 (more pronounced on the right), and from POLIMI results in Figure 20 (left), where the authority in terms of torsion per unit span per unit electric field of a patch starting at 10% of the chord and expanding up to 70% of the chord is shown. An “averaged” slope, illustrated in Figure 20 (right), has been obtained by moving a short MFC patch (roughly 3% of the chord) between 20% and 60% of the chord, crossing the end of the “C” spar at about 35% of the chord. The figure clearly shows that the MFC patch encounters a pronounced loss of authority in the vicin-

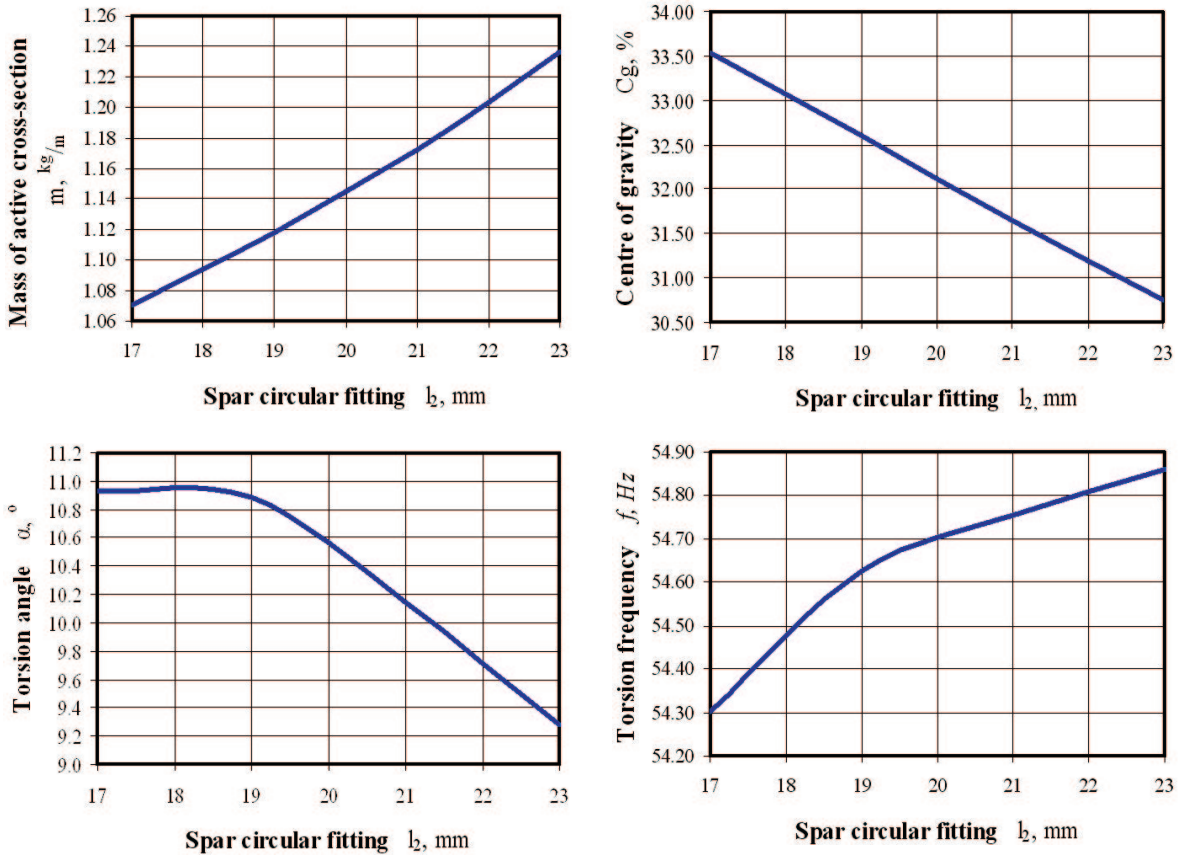


Figure 19: Dependence of mass (top, left), C.G. chordwise location (top, right), active twist (bottom, left) and 1<sup>st</sup> torsional frequency (bottom, right) on the chordwise position of the nose circular fitting.

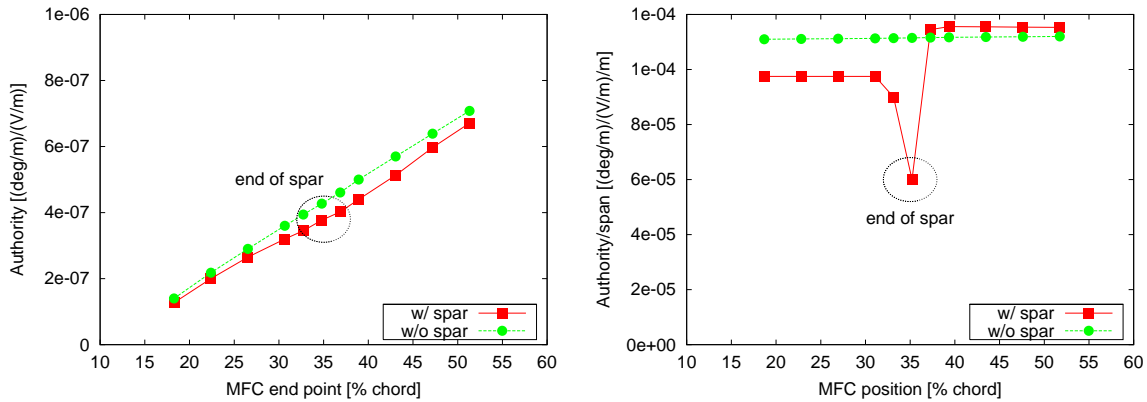


Figure 20: Dependence of induced torsion angle on MFC chordwise length (left) and position (right).

ity of the rear end of the “C” spar. This result was obtained with a relatively sharp “C” spar end; it is partially attenuated when a more regular blending, as the one illustrated in Figure I, is used. Moreover, the blade section layout illustrated in Figure 15, resulting from POLIMI’s optimization, is in agreement with the behavior observed by RTU in case (3) of Figure 17.

In fact, the rear end of the spar always tends to move towards the leading edge as much as possible, to leave the MFC patch outside the “C” spar region.

## Concluding Remarks and Future Prospects

This work describes the current status of the active twist rotor investigation that is part of the Friendcopter EU sponsored project. The participating partners set up and performed some preliminary parametric studies and constrained optimizations of an innovative configuration for an active twist blade section. Despite the use of rather heterogeneous analysis tools, the results agree quite well.

The insight provided by the parametric analysis and the preliminary optimizations indicates that the actuation authority increases if the MFC patches and the "C" spar overlap as little as possible. This requires to allow the distributed actuators to carry some significant portion of the bending and torsional loads, which may not be acceptable and needs further investigation. Furthermore, because of the considerable density of the piezoelectric fraction of the MFC, this placement results in having the C.G. in a rearward position that may give rise to aeroelastic issues.

Unless the design obtained with additional constraints, based on simple aeroelastic considerations, appear acceptable, a multi-level integrated aeroservoelastic optimization will be necessary for the continuation of the project.

## Acknowledgment

This work is partially supported by the EU project "Friendcopter", Contract no: AIP3-CT-2003-502773.

## References

- [1] Johannes Riemenschneider, Stefan Keye, Peter Wierach, and Hugues Mercier des Rochettes. Review of the common DLR/ONERA project active twist blade (ATB). In *30<sup>th</sup> European Rotorcraft Forum*, pages 22.1–9, Marseille, France, 14–16 September 2004.
- [2] William Keats Wilkie, Matthew L. Wilbur, Paul H. Mirick, Carlos E. S. Cesnik, and SangJoon Shin. Aeroelastic analysis of the NASA/Army/MIT active twist rotor. In *American Helicopter Society 55<sup>th</sup> Forum*, Montreal, Canada, May 25–27 1999.
- [3] K. Wilkie, R. G. Bryant, J. W. High, and J. A. Ligman. Free strain electromechanical characterization of the NASA macrofiber composite piezoceramic actuator. In *SPIE 2001*, volume 4333, New Port Beach, 2001.
- [4] P. Wierach and A. Schönecker. Design and application of piezocomposites in adaptronics. In *Adaptronic Congress 2005*, Göttingen, June 2005.
- [5] Gian Luca Ghiringhelli, Pierangelo Masarati, and Paolo Mantegazza. Characterisation of anisotropic, non-

homogeneous beam sections with embedded piezoelectric materials. *J. of Intell. Mat. Systems & Structures*, 8(10):842–858, October 1997.

- [6] Gian Luca Ghiringhelli, Pierangelo Masarati, and Paolo Mantegazza. Analysis of an actively twisted rotor by multibody global modelling. *Composite Structures*, 52/1:113–122, April 2001.
- [7] Evgeny Barkanov, Rolands Rikards, and Andris Chate. Numerical optimisation of sandwich and laminated composite structures. In M. El-Sayed S. Hernández and C. A. Brebbia, editors, *Structural Optimization, Proc. of Fourth International Conference on Computer Aided Optimum Design of Structures OPT195*, pages 311–318, Miami, Florida, USA, 19–21 September 1995. Computational Mechanics Publications, Southampton-Boston.